



# Liquefaction Hazard in the Groningen Region of the Netherlands due to Induced Seismicity

R. A. Green, M.ASCE<sup>1</sup>; J. J. Bommer<sup>2</sup>; P. J. Stafford<sup>3</sup>; B. W. Maurer, M.ASCE<sup>4</sup>; P. P. Kruiver<sup>5</sup>; B. Edwards<sup>6</sup>; A. Rodriguez-Marek, M.ASCE<sup>7</sup>; G. de Lange<sup>8</sup>; S. J. Oates<sup>9</sup>; T. Storck<sup>10</sup>; P. Omidj<sup>11</sup>; S. J. Bourne<sup>12</sup>; and J. van Elk<sup>13</sup>

**Abstract:** The operator of the Groningen gas field is leading an effort to quantify the seismic hazard and risk of the region due to induced earthquakes, including overseeing one of the most comprehensive liquefaction hazard studies performed globally to date. Due to the unique characteristics of the seismic hazard and the geologic deposits in Groningen, efforts first focused on developing relationships for a Groningen-specific liquefaction triggering model. The liquefaction hazard was then assessed using a Monte Carlo method, wherein a range of credible event scenarios were considered in computing liquefaction damage-potential hazard curves. This effort entailed the use of a regional stochastic seismic source model, ground motion prediction equation, site response model, and geologic model that were developed as part of the broader regional seismic hazard assessment. No to minor surficial liquefaction manifestations are predicted for most sites across the study area for a 2475-year return period. The only sites where moderate surficial liquefaction manifestations are predicted are in the town of Zandeweer, with only some of the sites in the town being predicted to experience this severity of liquefaction for this return period. **DOI: 10.1061/(ASCE)GT.1943-5606.0002286.** This work is made available under the terms of the Creative Commons Attribution 4.0 International license, <https://creativecommons.org/licenses/by/4.0/>.

## Introduction

The Groningen gas field is located in the northeastern region of the Netherlands and is one of the largest in the world. It has produced

over 2,000 billion m<sup>3</sup> of natural gas since the start of production in 1963. The first earthquakes linked to the gas production in the Groningen field occurred in December 1991, although earthquakes were linked to production at other gas fields in the region since 1986. To date, the largest induced earthquake linked to production at the Groningen field is the 2012 local magnitude ( $M_L$ ) 3.6 Huizinge event. However, the largest recorded peak ground acceleration (PGA: 0.11g) to date is associated with motions recorded during the January 8, 2018,  $M_L$  3.4 Zeerijp earthquake. In response to concerns about the induced earthquakes, the field operator Nederlandse Aardolie Maatschappij (NAM) is leading an effort to quantify the seismic hazard and risk resulting from the gas production operations (van Elk et al. 2017, 2019). Because of the widespread deposits of saturated sands in the region, the risk due to liquefaction triggering was evaluated as part of this effort. Although an almost negligible contributor to earthquake fatalities (e.g., Hakuno 2004; Green and Bommer 2019), liquefaction triggering and associated phenomena are important threats to the built environment and in particular to infrastructure and lifelines (e.g., Bird and Bommer 2004).

The 2017 version of the Netherlands' National Annex to the Eurocode 8 [NPR 9998 (NPR 2017)] details requirements for assessing the impact of liquefaction and related phenomena and recommends the use of the Idriss and Boulanger (2008) simplified model (IB08) for predicting liquefaction triggering. However, as detailed in Green et al. (2019), the suitability of this model in Groningen is questionable, as is any other existing simplified model. This is because simplified models are semiempirical, with the empirical aspects having been developed primarily for tectonic earthquakes in active shallow-crustal tectonic regimes (e.g., California, Japan, and New Zealand). The seismic hazard and the geologic profiles/soil deposits in Groningen differ significantly from those where existing models were developed. Specifically, and as detailed in subsequent sections of this paper, the suitability of the depth-stress reduction factor ( $r_d$ ) and magnitude scaling factor (MSF) relationships inherent to existing models are uncertain for

<sup>1</sup>Professor, Dept. of Civil and Environmental Engineering, Virginia Tech, Blacksburg, VA 24061 (corresponding author). ORCID: <https://orcid.org/0000-0002-5648-2331>. Email: [rugreen@vt.edu](mailto:rugreen@vt.edu)

<sup>2</sup>Senior Research Investigator, Dept. of Civil and Environmental Engineering, Imperial College London, London SW7 2AZ, UK. ORCID: <https://orcid.org/0000-0002-9709-5223>

<sup>3</sup>Reader, Dept. of Civil and Environmental Engineering, Imperial College London, London SW7 2AZ, UK.

<sup>4</sup>Assistant Professor, Dept. of Civil and Environmental Engineering, Univ. of Washington, Seattle, WA 98195.

<sup>5</sup>Senior Geophysicist, Deltares, P.O. Box 177, 2600 MH, Delft, The Netherlands. ORCID: <https://orcid.org/0000-0003-0409-3542>

<sup>6</sup>Senior Lecturer, School of Environmental Sciences, Univ. of Liverpool, Liverpool L69 3GP, UK.

<sup>7</sup>Professor, Dept. of Civil and Environmental Engineering, Virginia Tech, Blacksburg, VA 24061. ORCID: <https://orcid.org/0000-0002-8384-4721>

<sup>8</sup>Senior Engineering Geologist, Deltares, P.O. Box 177, 2600 MH, Delft, The Netherlands.

<sup>9</sup>Principal Geophysicist, Shell Global Solutions International B.V., P.O. Box 60, 2280 AB, Rijswijk, The Netherlands.

<sup>10</sup>Consultant Simulation and Modeling, Alten, Capelle a/d IJssel, Fascinatou Boulevard 582, 2909 VA, Capelle aan den, IJssel, The Netherlands.

<sup>11</sup>Consultant Simulation and Modeling, Alten, Capelle a/d IJssel, Fascinatou Boulevard 582, 2909 VA, Capelle aan den, IJssel, The Netherlands.

<sup>12</sup>Senior Principal Science Expert Earth Sciences, Shell Global Solutions International B.V., Grasweg 31, 1031 HW, Amsterdam, The Netherlands. ORCID: <https://orcid.org/0000-0003-2925-8411>

<sup>13</sup>Development Lead Groningen Asset, Nederlandse Aardolie Maatschappij B.V. (NAM), Schepersmaat 2, 9405 TA, Assen, The Netherlands.

Note. This manuscript was submitted on July 19, 2019; approved on February 5, 2020; published online on June 12, 2020. Discussion period open until November 12, 2020; separate discussions must be submitted for individual papers. This paper is part of the *Journal of Geotechnical and Geoenvironmental Engineering*, © ASCE, ISSN 1090-0241.



liquefaction hazards [i.e., assessing the liquefaction triggering potential for a ground motion having a 2475-year return period, e.g., Korff et al. (2019)]. Additionally, the integration of the liquefaction hazard study within the broader regional seismic hazard study resulted in one of the most comprehensive liquefaction hazard studies performed globally to date, due to the development and use of a regional stochastic source model, ground motion prediction equation (GMPE), site response model, and geologic model, as well as the region-specific liquefaction triggering model.

## Background

Tectonic seismicity in the Netherlands is primarily associated with the Roer Valley graben in the southeast of the country (Fig. 2), where the Roer Valley graben was the source of the largest earthquake known to have occurred in the Netherlands, the moment

magnitude,  $M$ , 5.8 April 13, 1992 Roermond earthquake (Trifonov et al. 1994). In contrast, induced seismicity resulting from natural gas production mostly occurs in the northern portion of the country, including seismicity resulting from gas production in the Groningen field. This regional gas reservoir exists within the Slochteren-Rotliegend sandstone at a depth of about 3 km; it is overlain by the Zechstein salt layer, an ~1-km thick layer of chalk, and then the North Sea Formation (Fig. 3). The seismicity resulting from production at the Groningen field from 1996 to 2019 is shown in Fig. 4. Based on projected gas production rates from 2016 to 2021, motions having a 2475-year return period are predicted to have PGAs up to approximately 0.21g (van Elk et al. 2017), with the dominant contributions from  $M$  4.0–5.5 events.

The velocity model for the entire gas field from the ground surface down to the base of the North Sea Supergroup (designated henceforth as NS\_B) is described in detail by Kruiver et al. (2017a, b). The NS\_B horizon has an average depth of ~800 m

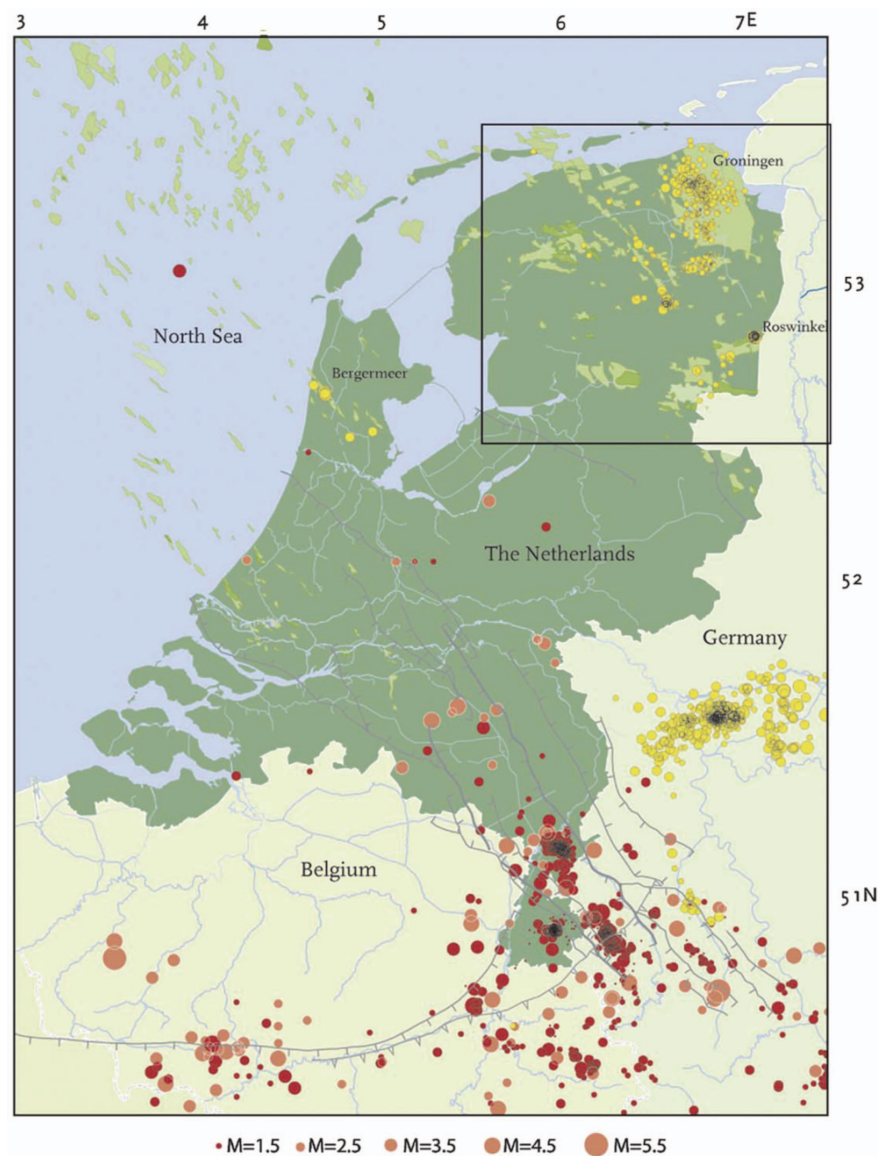


**Fig. 2.** (Color) General overview of the seismicity in the Netherlands and its immediate surroundings from 1900 to 2006. Red circles indicate natural tectonic earthquakes. Yellow circles indicate earthquakes caused by man-made activities, classified by The Royal Netherlands Meteorological Institute (KNMI), usually mining or gas exploitation. The circles are scaled according to earthquake magnitude. Gray solid lines indicate mapped faults in the upper-North Sea formation based on data from TNO Geoscience. Light green indicates the approximate contours of the gas fields. (Reproduced from van Eck et al. 2006, with permission from Elsevier.)

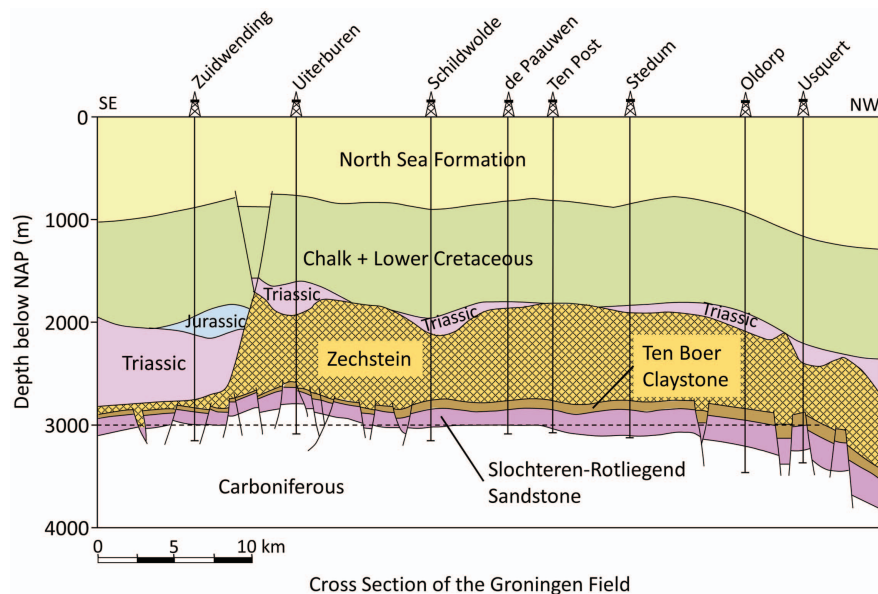


**Fig. 3.** (Color) Geologic cross section through the Groningen gas field (reproduced from Rodriguez-Marek et al. 2017, with permission from the Seismological Society of America). The regional gas reservoir exists within the Slochteren-Rotliegend sandstone at a depth of about 3 km. NAP = Dutch Ordnance Datum.

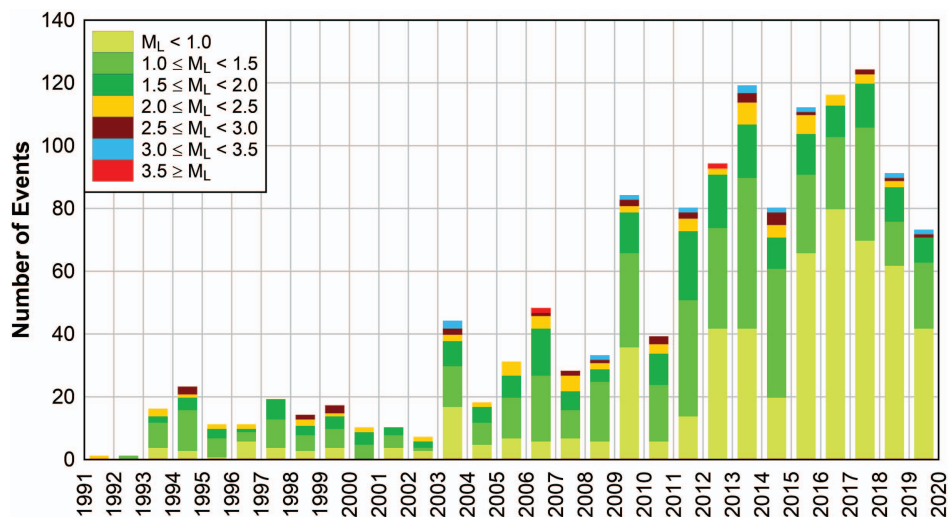


**Fig. 4.** (Color) Number of events occurring within the Groningen gas field as a function of time and  $M_L$  from December 5, 1991 to October 18, 2019. (Data from NAM 2019.)

across the Groningen field and is the first elevation at which a strong and persistent velocity contrast is encountered. The velocity model from the ground surface to 50 m below the Dutch Ordnance Datum is based on a geostatistical model (i.e., the GeoTOP model) that has a  $100 \times 100$  m spatial resolution that assigns a stratigraphic unit and a lithological class to 0.5-m thick voxels (Stafleu et al. 2011). The GeoTOP model correlates each stratigraphic lithological unit to soil parameters (mean and standard deviation). These parameters include small-strain shear wave velocity ( $V_S$ ), soil density, coefficients of uniformity, median grain-size diameter, cone penetration test (CPT) tip resistance ( $q_c$ ), and undrained shear strength. When observed, the depth dependence of  $V_S$  is included in these correlations. Independent measurements of the near-surface  $V_S$  profiles at accelerograph recording stations showed the GeoTOP-derived profiles to be accurate (Noorlandt et al. 2018). For depths greater than 50 m, velocities are assigned from the

analysis of surface waves collected in field-wide seismic reflection surveys of the Groningen gas reservoir. These measurements extend the  $V_S$  profile to a depth of about 120 m and are described in more detail in Kruiver et al. (2017a, b). Below this depth, measurements from sonic logs in the field are used to extend the profiles to the NS\_B reference horizon (Kruiver et al. 2017a, b). The uncertainty in  $V_S$  for depths greater than about 50 m is ignored because it was determined that these uncertainties have little impact on computed site response. The unit weights for the various stratigraphic lithological units are estimated by correlations with CPT from Lunne et al. (1997). For some of the deeper formations, the unit weights are assumed to be constant, consistent with the logs from two deep boreholes (Kruiver et al. 2017a, b). The NS\_B and underlying strata have  $V_S$  of  $\sim 1.5$  km/s and a unit weight of  $\sim 21$  kN/m<sup>3</sup>. An example of the resulting  $V_S$  profiles from the field-wide velocity model is shown in Fig. 5.

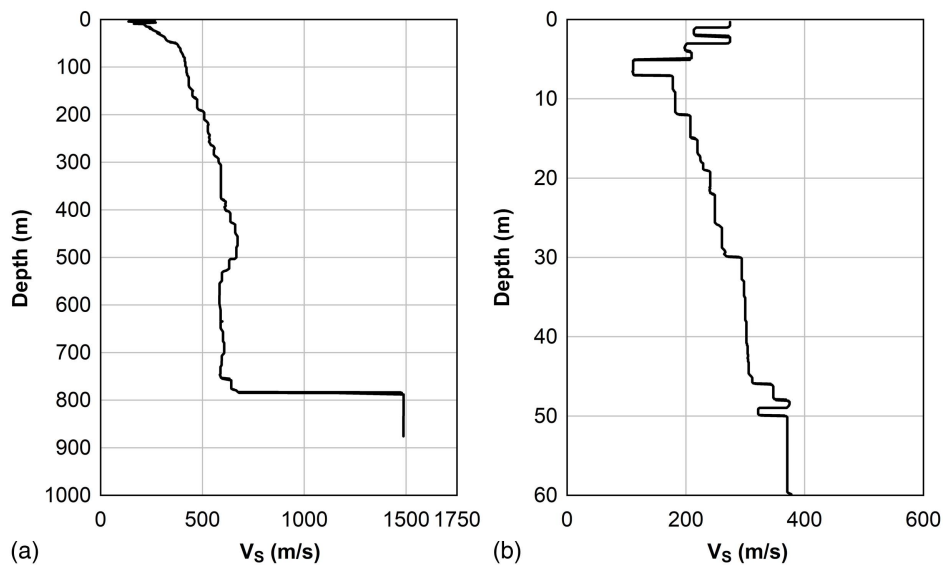


**Fig. 5.** Example  $V_s$  profile at the location of ground-motion recording station G09: (a) full profile down to NS\_B; and (b) enlarged view of the upper 60 m of the profile. (Rodriguez-Marek et al. 2017.)

As mentioned in the Introduction, the stress-based simplified liquefaction triggering model is central to the liquefaction hazard/risk assessment of the Groningen field. The revised model proposed by Green et al. (2019) is a modification of the Boulanger and Idriss (2014) model, which in turn is an update of the model recommended by NPR 9998-2017 (i.e., Idriss and Boulanger 2008). The modifications proposed by Green et al. (2019) were prompted by potential biases in the  $r_d$  and MSF relationships inherent to the Boulanger and Idriss (2014) procedure, with these relationships accounting for the nonrigid response of the soil column during earthquake shaking and the influence of strong ground motion duration on liquefaction triggering. However, given the semiempirical approach used to develop the liquefaction triggering curves (or cyclic resistant ratio, CRR, curves), alternative  $r_d$  and MSF relationships cannot simply be used in conjunction with a CRR curve that was developed using other  $r_d$  and MSF relationships (NRC 2016). Rather, the new  $r_d$  and MSF relationships, along with other needed relationships, must be used to analyze the compiled liquefaction/no liquefaction case histories and a new CRR curve must be regressed. Green et al. (2019) did this using the  $r_d$  relationship proposed by Lasley et al. (2016) and an MSF that they developed using the number of equivalent cycles ( $n_{eq}$ ) correlation proposed by Lasley et al. (2017). Both of these relationships are for shallow-crustal events in active tectonic settings, consistent with the liquefaction/no liquefaction case histories analyzed.

## Groningen-Specific $r_d$ , $n_{eq}$ , and MSF Relationships

### Geologic Profiles

As mentioned previously, Groningen-specific  $r_d$ ,  $n_{eq}$ , and MSF needed to be developed following the approaches used by Lasley et al. (2016, 2017) and Green et al. (2019) to develop the revised  $r_d$ ,  $n_{eq}$ , and MSF for tectonic earthquakes. This allows the Groningen-specific relationships to be used in conjunction with the CRR curve developed by Green et al. (2019). Accordingly, a series of site response analyses needed to be performed using region-specific ground motions and geologic profiles. The GeoTOP model was used to develop profiles for use in the site response analyses.

The NS\_B was chosen as the reference rock horizon and was treated as the top of the elastic half-space in the site response analyses performed in this study (Rodriguez-Marek et al. 2017). Although another velocity contrast is encountered at a depth of  $\sim 400$  m at the Brussels Sands formation, a velocity reversal occurs at a depth of  $\sim 500$  m that is inconsistent with the properties of an elastic half-space and thus prevents the top of the Brussels Sands formation from being used as the reference horizon. Moreover, the Brussels Sands formation is not consistently mapped across the entire field; in contrast, the NS\_B is well defined over the entire study area.

The liquefaction study area shown in Fig. 6 crosses over several zones used to develop site amplification factors for the region (Rodriguez-Marek et al. 2017); for the most part, the site amplification zones coincide with the geological zonation presented in Kruiver et al. (2017a). From NW to SE, the liquefaction study area crosses over zones 821, 801, 603, 604, 1001, 602, 1032, and 2001. Given that  $r_d$ ,  $n_{eq}$ , and MSF relationships are functions of the response characteristics of a geologic profile, separate relationships were developed for each of the site amplification zones within the liquefaction study area. Additionally, previous studies raised concerns about the liquefaction hazard in the downtown region of Zandweer (Kumar 2017), which lies within the liquefaction study area. As a result, this region was treated as a separate zone.

In selecting sites used to develop the Groningen-zone-specific  $r_d$ ,  $n_{eq}$ , and MSF relationships, preference was given to sites that were characterized by CPT; the locations of the CPT soundings within the study area that were available at the start of this study are shown in Fig. 6(b). For each CPT, the corresponding profile realization (i.e., GeoTOP voxel stack) in which the sounding was performed was identified. In several cases, two or more soundings were performed within the same  $100 \times 100$  m GeoTOP voxel stack. If the number of unique GeoTOP voxel stacks in which the CPT soundings were performed in a zone was less than ten, then additional GeoTOP voxel stacks were chosen to ensure that at least ten unique GeoTOP voxel stacks per zone were used in this study. The locations of these additional GeoTOP voxel stacks were selected to ensure a relatively uniform spatial distribution across a zone. Also, if the number of unique GeoTOP voxel stacks in which the CPT soundings were performed in a zone was at least ten but

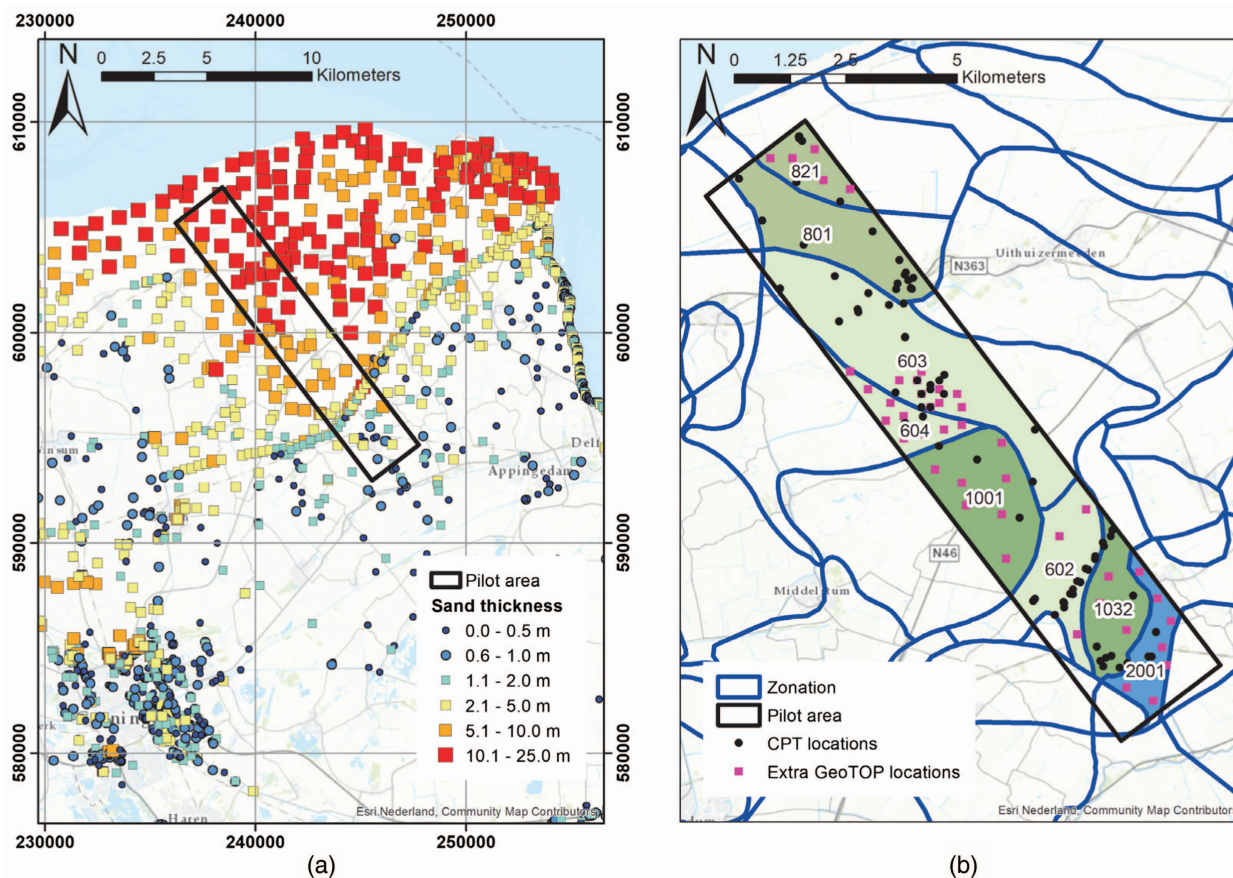


**Fig. 6.** (Color) Location of the liquefaction study area across the Groningen gas field: (a) cumulative thicknesses (m) of the Holocene sand deposits that comprise the Naaldwijk formation; and (b) site amplification zones, locations of CPT soundings, and the locations of additional GeoTOP voxel stack profiles used in the site response analyses to generate Groningen-zone-specific  $r_d$ ,  $n_{eq}$ , and MSF relationships. (© Esri Nederland, Community Map Contributors.)

**Table 1.** Number of geologic profiles per zone used in the site response analyses to develop Groningen-zone-specific  $r_d$ ,  $n_{eq}$ , and MSF relationships

Zone	Number of profiles
602	16
603	12
604	10
801	11
821	10
1001	10
1032	15
2001	10
Zandweer	16
Total	110

the spatial distribution of these stacks was not relatively uniform across the zone, three additional GeoTOP voxel stacks were chosen for that zone. The locations of the additional GeoTOP voxel stack profiles used in the site response analyses are shown in Fig. 6(b) and listed as “Extra GeoTOP locations” in the figure legend. The numbers of profiles per zone are listed in Table 1, with a total of 110 profiles across the liquefaction study area used to develop the zone-specific  $r_d$ ,  $n_{eq}$ , and MSF relationships.

### Ground Motions

The ground motions at the NS\_B reference horizon used in the site response analyses to develop the Groningen-zone-specific  $r_d$ ,  $n_{eq}$ ,

and MSF relationships were generated using finite-fault, stochastic simulation using the EXSIM code (Motazedian and Aktinson 2005; Boore 2009). Each of the distributed subfaults in this technique is assumed to be a point source (effectively a small magnitude earthquake) and can be characterized using the seismological parameters observed in events recorded in the Groningen gas field. This process is detailed by Bommer et al. (2017b) and Edwards et al. (2019) and briefly summarized in the following section.

The first stage in calibrating the source model is to transform the surface recordings to the NS\_B reference horizon, central to which is the velocity model from the NS\_B horizon to the ground surface discussed previously. The Fourier amplitude spectra (FAS) from the surface and from 200-m boreholes were transformed to the NS\_B horizon using a one-dimensional transfer function, as implemented in the site response software STRATA (Kottke and Rathje 2008). Because the motions recorded to date are very weak (i.e.,  $M_L$  2.5 to 3.6 and distances from 0 to 20 km), the near-surface layers were assumed to have responded essentially linearly to the excitations; therefore, the deconvolution was made assuming linear site response. Linear amplification factors were also calculated for the response spectra using the random vibration theory (RVT) procedure implemented in STRATA. The factors were calculated for the same  $V_S$ , damping, and unit weight profiles, with input motions at the NS\_B obtained from simulations, using an earlier version of the model. The amplification factors for the response spectra were found to be scenario-dependent (Stafford et al. 2017).

The FAS at the NS\_B horizon were then inverted, following the approach of Edwards et al. (2019), for source, path, and site

parameters. Three parameters were then fitted to each FAS: the event-specific source corner-frequency ( $f_0$ ) of a parametric source spectrum (e.g., Brune 1970; Boatwright 1978), record-specific signal moment (long-period spectral displacement plateau), and high-frequency attenuation term, kappa ( $\kappa$ ). As a result of the relatively small dataset of recorded motions available for these inversions, some elements were constrained independently. First,  $\kappa$  was estimated from individual FAS plotted on log-linear axes following Anderson and Hough (1984). Second, the form of the geometric spreading was obtained from full waveform finite difference simulations performed using a 3D velocity model for the field. The inversions were then used to estimate the stress parameter ( $\Delta\sigma$ ), decay rates in each segment, quality factor (Q) value, and amplification factor at the NS\_B (which was found to be close to 1). For the inversions, the use of both the Brune (1970) and Boatwright (1978) spectra was explored, and because neither performed consistently better, the former was used.

Based on the geometric spreading model and the results of the inversions of the FAS, many combinations of  $\Delta\sigma$ , Q, and site kappa ( $\kappa_0$ ) were explored to identify the combination of parameters that best fit the response spectral ordinates at the NS\_B horizon. The duration model used to link the FAS and response spectral ordinates was an empirically-based Groningen-specific model (Bommer et al. 2016). The model that best fit the motions at the NS\_B horizon in this case had a  $\Delta\sigma$  of 60 bar, frequency independent Q of 200, and  $\kappa_0$  of 0.015 s, which were then used in forward simulations.

The software EXSIM (Boore 2009, based on Motazedian and Atkinson 2005) was used in conjunction with the Groningen-specific stochastic point source model parameters to generate motions at the NS\_B for magnitudes ranging from  $M$  3.5 to 7.0, with  $\Delta M = 0.5$ , and horizontal distances to the fault center (R) ranging from 0.1 to 60 km, with  $\Delta \log(R) = 0.2$ , resulting in a total of 120 magnitude-distance combinations. Each M-R scenario was recorded at eight azimuths radially around the center of the strike of the finite fault, leading to 960 motions. Fault dimensions were based on Wells and Coppersmith (1994) for  $M > 5$ , otherwise, Brune (1970), with each event sampling one realization of the distribution (with a standard deviation of 0.15 log-units) of possible fault dimensions. Hypocenters were randomly located along strike, but always at  $z = 3$  km (the reservoir depth), with propagation downwards (at  $0.8\beta$  with 50% subfault pulsing) until the seismogenic depth of 13 km. For larger events, fault ruptures then grow horizontally, bounded by the reservoir and the seismogenic depth. Subfault durations were sampled from the Bommer et al. (2016) duration model, accounting for between- and within-event variability. The maximum magnitude of  $M$  7.0 was determined by an expert panel (Bommer and van Elk 2017). In extrapolating to magnitudes so much larger than the largest recorded event ( $M$  3.6), the inevitable epistemic uncertainty in the generated motions for larger magnitude events needed to be considered. This was performed by both introducing magnitude-dependence of  $\Delta\sigma$  into the model and also creating alternative (higher and lower) models, as had been done previously (Bommer et al. 2017b). The weights assigned to these branches are 0.1 for the lower branch since it is unclear whether low stress drop values would persist at larger magnitudes and 0.3 each to the two central and upper models. In total, 3840 motions were generated and used in the site response analyses to develop the Groningen-zone-specific  $r_d$ ,  $n_{eq}$ , and MSF relationships.

### Regression Analysis

In total, 422,400 site response analyses were performed to develop Groningen-zone-specific  $r_d$ ,  $n_{eq}$ , and MSF relationships

(110 profiles  $\times$  3,840 motions = 422,400 analyses). The site response analyses were performed using the equivalent linear code, ShakeVT2 (Thum et al. 2019), which outputs  $r_d$  and  $n_{eq}$  values for the liquefiable layers, directly, for each analysis as a function of depth in the profile. The depth range considered for the regression analyses was restricted to 20 m and shallower. The reason for this was twofold. First, the scaling of  $r_d$  was very stable over this depth range, and including more data for deeper depths only acted to negatively influence the regression fit over the 0–20 m depth range. Second, and more importantly, liquefaction is a near-surface phenomenon and none of the compiled liquefaction case history databases (e.g., Cetin 2000; Moss et al. 2003; Kayen et al. 2013; Boulanger and Idriss 2014) include cases deeper than 20 m. The regression analyses were performed on well over 1,000,000 data points.

### Groningen-Zone-Specific $r_d$ Relationships

For ease of model development, ease of implementation, and consistency with previous work, a relatively simple regression approach was used to develop the Groningen-zone-specific  $r_d$  relationships. Traditional nonlinear least-squares regression could not be used because of the complicated heteroscedastic standard deviation (i.e., the standard deviation is a function of the predictor variables: depth,  $z$ , and moment magnitude,  $M$ ). Therefore, maximum likelihood estimation was used directly and error estimates for each parameter were obtained from the Hessian matrix of the likelihood function (i.e., negative of the second derivative of the logarithm of the likelihood function).

Several functional forms were considered during the model development, including the functional form adopted in the worldwide model developed by Lasley et al. (2016). The final functional form was based upon a sigmoid shape with the main variable being logarithmic depth. However, the location and scale parameters of the sigmoid are functions of  $M$ ,  $V_S$ , and  $a_{max}$  (i.e., PGA at the surface of the soil profile). There is an apparent break in scaling for relatively large values of  $a_{max}$ ; consequently, this effect was modeled. The dependence on the time-weighted average  $V_S$  of the upper 12 m of the profile ( $V_{S12}$ ) that was included in the worldwide  $r_d$  relationship developed by Cetin (2000) was also observed in the Groningen data and was thus included in the relationships developed herein. The same functional form of the regression equation was used for all zones, and the regression coefficients were found to be statistically significant in all cases. The final functional form was selected based on likelihood ratio tests performed on the alternative models considered.

The final functional form for  $r_{d-Gron}$  is

$$r_{d-Gron} = 1 - \frac{A_{rd}}{1 + \exp\left[-\frac{\ln(z) - (\beta_2 + \beta_6 \cdot M)}{(\beta_3 + \beta_7 \cdot M)}\right]}; \quad 0 \leq r_d \leq 1 \quad (1a)$$

where  $z$  has units of m;  $\beta_i$  = regression coefficients (Table 2); and  $A_{rd}$  = Eq. (1b) and (1c) and represents the asymptotic level for  $r_{d-Gron}$  at depth (that is,  $r_{d-Gron} = 1 - A_{rd}$  as  $z \rightarrow \infty$ ).

$$A_{rd} = \beta_1 + \beta_4 \cdot \min[M, 6.5] + \beta_5 \cdot \ln(a_{max}) + \beta_9 \cdot V_{s12}; \quad \text{for } a_{max} \leq 0.3g \quad (1b)$$

$$A_{rd} = \beta_1 + \beta_4 \cdot \min[M, 6.5] + \beta_5 \cdot \ln(a_{max}) + \beta_8 \cdot \ln\left(\frac{a_{max}}{0.3}\right) + \beta_9 \cdot V_{s12}; \quad \text{for } a_{max} > 0.3g \quad (1c)$$

where  $a_{max}$  is in units of  $g$ ; and  $V_{S12}$  is in units of m/s.

**Table 2.** Regression coefficients for the  $r_{d-Gron}$  model

Zone	$\beta_1$	$\beta_2$	$\beta_3$	$\beta_4$	$\beta_5$	$\beta_6$	$\beta_7$	$\beta_8$	$\beta_9$	$\beta_{10}$
602	2.0845	1.1474	0.9709	-0.2080	0.0744	0.1148	-0.0882	0.2707	-0.0020	0.1520
603	2.1200	1.0467	0.6685	-0.2039	0.0800	0.1374	-0.0328	0.5033	-0.0024	0.1575
604	2.1687	1.2050	0.8968	-0.2205	0.0816	0.0629	-0.0738	0.4258	-0.0021	0.1443
801	2.5725	1.1450	0.4983	-0.2296	0.0734	0.1634	0.0437	0.7463	-0.0041	0.1908
821	2.7957	1.5813	0.9813	-0.2732	0.1003	0.0599	-0.0743	0.4674	-0.0039	0.1889
1001	2.1226	1.0583	0.7360	-0.2024	0.0722	0.1305	-0.0561	0.4349	-0.0032	0.1570
1032	1.7208	0.8872	0.4872	-0.1697	0.0638	0.1247	-0.0189	0.4720	-0.0017	0.1465
2001	2.2369	1.1288	0.8699	-0.2019	0.0772	0.1322	-0.0285	0.4831	-0.0030	0.1629
Zandeweer	2.4832	1.1972	0.8834	-0.2194	0.0772	0.1472	-0.0662	0.4002	-0.0037	0.1405

The model also has a heteroscedastic standard deviation that is defined by

$$\sigma_{r_d} = \frac{\beta_{10}}{1 + \exp\left[-\frac{\ln(\max\{z, 5\}) - (\beta_2 + \beta_6 \cdot \mathbf{M})}{(\beta_3 + \beta_7 \cdot \mathbf{M})}\right]} \quad (1d)$$

where  $z$  is in units of m; and  $\beta_i$  = regression coefficients (Table 2). Note that in Eq. (1d) the depth is defined as the maximum of the actual depth,  $z$ , and 5 m to prevent the standard deviation from becoming too small at very shallow depths.

The residual plots against the predictor variables used in Eq. (1) are shown in Fig. 7 for Zone 602, as an example. The very large number of residuals for each analysis case poses challenges

because small deviations are statistically significant and can lead to over-fitting. Therefore, in fitting the model, we focused on the main trends that were observed. The binned residuals are shown in Fig. 7 to better illustrate the center and the variance of the data. For example, in Fig. 7(a), there is a larger deviation of the data from the center near  $\log(a_{\max}) = -1$  from the residuals, but the binned residuals show that there is not significantly more variance here, but rather, it is just that there is such a large sample that more points are seen in the tails of the distribution. Additionally, it is important to note that the residual plots do not show any clear trends against the variables shown; thus, the model appears to capture the location-specific scaling of  $r_d$  well.

Fig. 8 shows a comparison of the Groningen-specific  $r_d$  relationship for Zone 602, as an example, and the worldwide  $r_d$

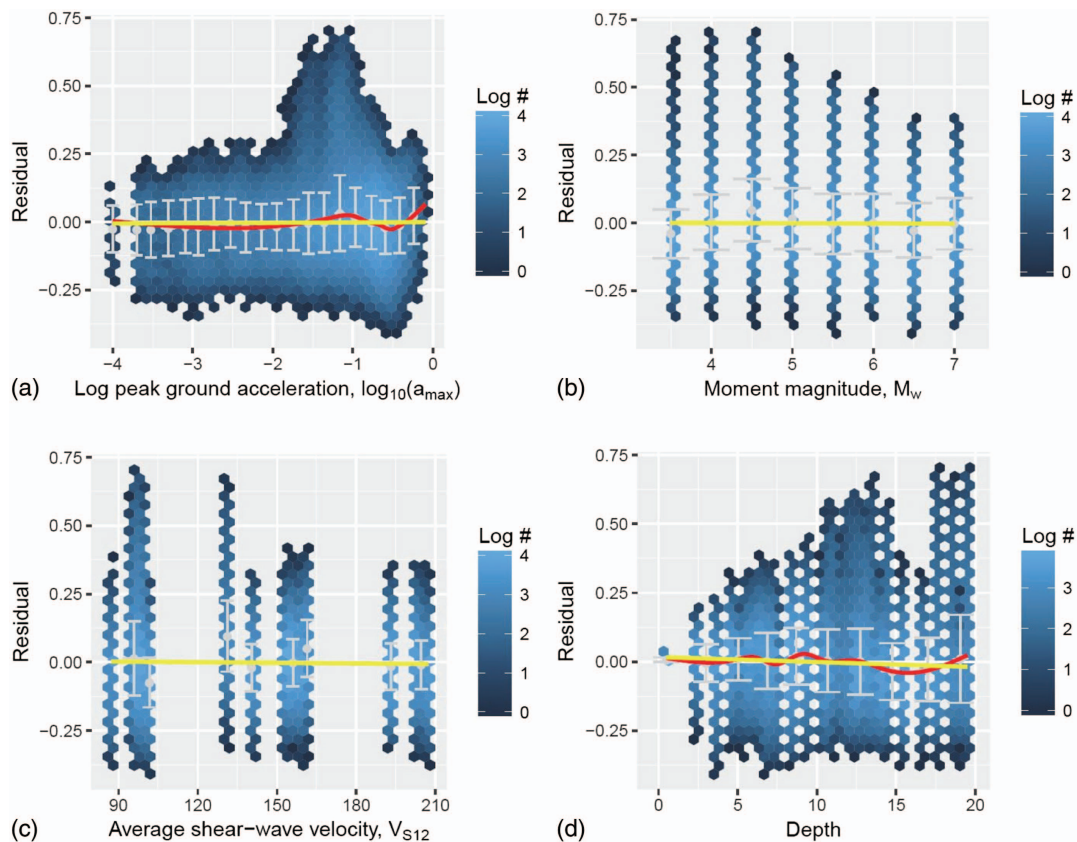


**Fig. 7.** (Color) Residuals of the  $r_{d-Gron}$  model for predictor variables for Zone 602 used in Eq. (1): (a) logarithm of  $a_{\max}$ ; (b) moment magnitude; (c) average small-strain shear-wave velocity of the upper 12 m of a profile,  $V_{S12}$ ; and (d) depth. Red lines show locally estimated scatterplot smoothing (LOESS) fits to the residuals, yellow lines show linear trends fitted to the residuals, and the light gray error bars show the means and standard deviations of residuals grouped into bins. Residuals are represented by color-coded hexagonal cells, with the color scaling in proportion to the logarithmic count of residuals in each hexagonal cell.

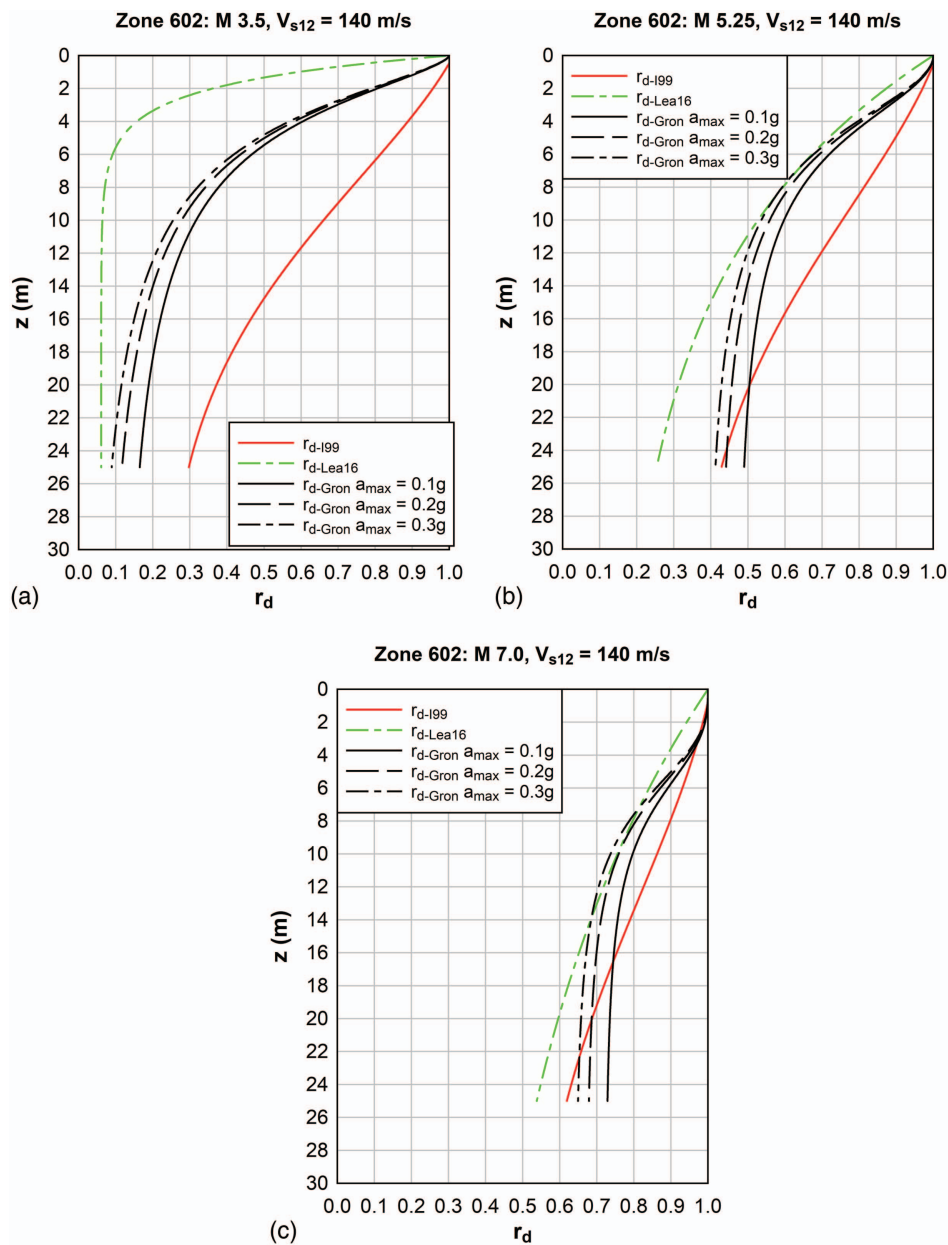


**Fig. 8.** (Color) Comparison of  $r_d$  relationships proposed by Idriss (1999) (I99), Lasley et al. (2016) (Lea16), and Groningen-specific relationship ( $r_{d-Gron}$ ) for Zone 602 for: (a)  $M$  3.5; (b)  $M$  5.25; and (c)  $M$  7.0. Because  $r_{d-Lea16}$  and  $r_{d-Gron}$  are functions of  $V_{S12}$ , a representative value for the liquefaction study area of 140 m/s was assumed for the plots. Additionally, because  $r_{d-Gron}$  is also a function of  $a_{max}$ , curves for  $a_{max} = 0.1, 0.2,$  and  $0.3g$  are shown in the plots.

relationships proposed by Idriss (1999) (adopted by both Idriss and Boulanger 2008; Boulanger and Idriss 2014) and Lasley et al. (2016). As may be observed from this figure, for small magnitude events (e.g.,  $M$  3.5), the Idriss (1999) and Lasley et al. (2016) relationships significantly overpredict and underpredict, respectively,  $r_d$  for the Groningen liquefaction study area. However, the lack of accuracy of these relationships for  $M$  3.5 is not altogether surprising because their intended use was for  $M \sim 5.0$  and greater. For moderate-sized events (e.g.,  $M$  5.25), there is still a general trend for the Idriss (1999) and Lasley et al. (2016) relationships to respectively overpredict and underpredict  $r_d$ , albeit not significantly so, with the Lasley et al. (2016) relationship providing more accurate predictions for the Groningen region than the Idriss (1999) relationship. For large magnitude events (e.g.,  $M$  7.0), the three  $r_d$  relationships predict similar values, with the general trend for the

Idriss (1999) and Lasley et al. (2016) relationships to respectively overpredict and underpredict  $r_d$  still persisting but at a much less significant level.

#### Groningen-Zone-Specific $n_{eq}$ and MSF Relationships

The functional form for the Groningen-zone-specific  $n_{eq}$  relationship is a slight modification of the worldwide model developed by Lasley et al. (2017), with the modifications made to reflect a clear break in scaling at large values of  $a_{max}$  and to include the observed dependence on  $V_{S12}$ . The functional form for the Groningen-zone-specific  $n_{eq}$  relationship is

$$\ln[n_{eqM-Gron}(M, a_{max}, V_{s12})] = \alpha_1 + \alpha_2 \cdot \ln(a_{max}) + \alpha_4 \cdot M + \alpha_5 \cdot V_{s12}; \quad \text{for } a_{max} \leq 0.3g \quad (2a)$$

**Table 3.** Regression coefficients for the  $n_{eqM-Gron}$  model

Zone	$\alpha_1$	$\alpha_2$	$\alpha_3$	$\alpha_4$	$\alpha_5$	$\sigma_{\ln(neqM-Gron)}$
602	-0.2732	-0.3001	-0.8100	0.1996	0.0038	0.4373
603	-0.0097	-0.2721	-0.4491	0.1351	0.0037	0.4708
604	-0.1018	-0.2966	-0.0192	0.1612	0.0038	0.4662
801	0.3877	-0.3213	-0.0984	0.1620	-0.0007	0.4575
821	-0.3764	-0.3080	-0.2753	0.1634	0.0045	0.4571
1001	-0.1958	-0.3246	-0.6973	0.1583	0.0033	0.4314
1032	-0.2487	-0.3131	-0.4085	0.1766	0.0038	0.4446
2001	-0.4359	-0.2936	-0.0154	0.1934	0.0052	0.4498
Zandeweer	0.6419	-0.3025	-0.7874	0.1829	-0.0017	0.4453

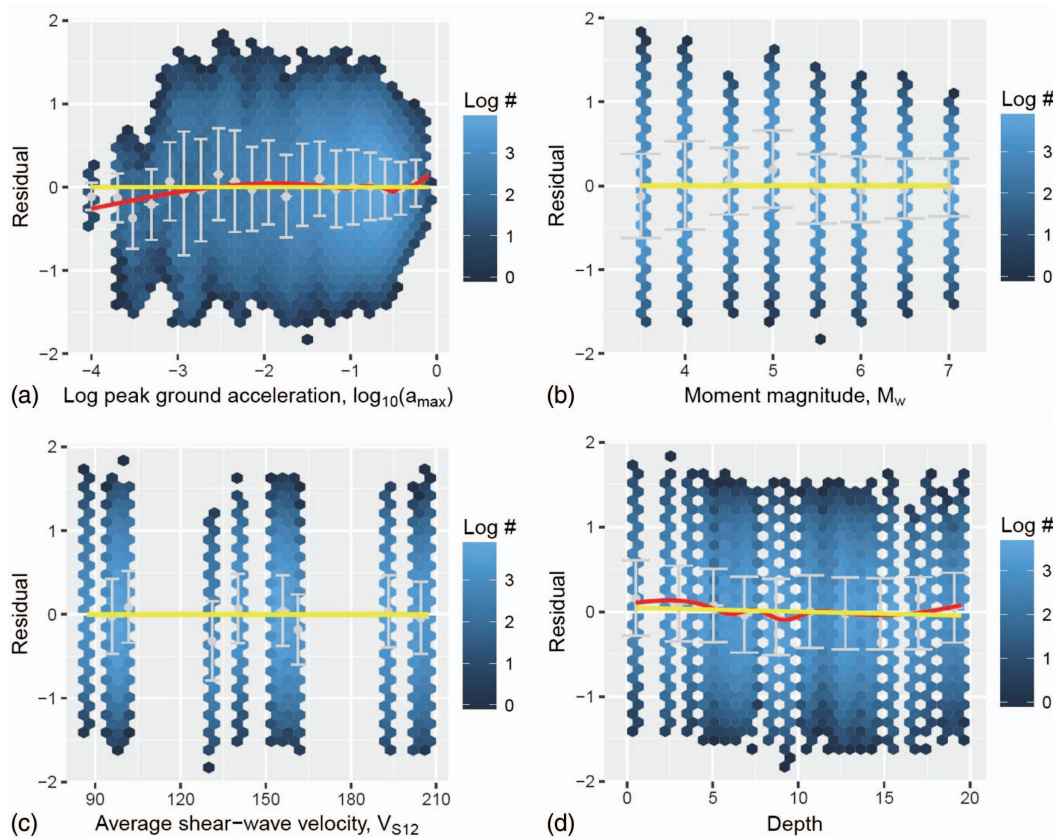


**Fig. 9.** (Color) Residuals of the  $n_{eqM}$  model for predictor variables for Zone 602 used in Eq. (2): (a) logarithm of  $a_{max}$ ; (b) moment magnitude; (c) average small-strain shear-wave velocity of the upper 12 m of a profile,  $V_{S12}$ ; and (d) depth. Red lines show locally estimated scatterplot smoothing (LOESS) fits to the residuals, yellow lines show linear trends fitted to the residuals, and the light gray error bars show the means and standard deviations of residuals grouped into bins. Residuals are represented by color-coded hexagonal cells, with the color scaling in proportion to the logarithmic count of residuals in each hexagonal cell.

$$\ln[n_{eqM-Gron}(M, a_{max}, V_{S12})]$$

$$= \alpha_1 + \alpha_2 \cdot \ln(a_{max}) + \alpha_3 \cdot \ln\left(\frac{a_{max}}{0.3}\right) + \alpha_4 \cdot M + \alpha_5 \cdot V_{S12};$$

for  $a_{max} > 0.3g$  (2b)

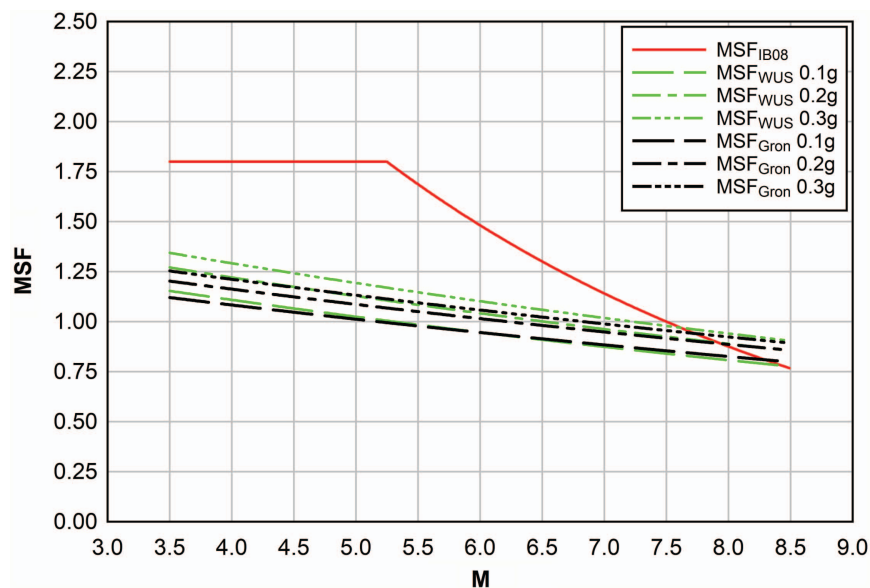
where  $a_{max}$  is in units of  $g$ ;  $V_{S12}$  is in units of  $m/s$ ;  $\alpha_i$  = regression coefficients (Table 3); and  $\sigma_{\ln(neqM)}$  for each zone is listed in the last column of Table 3. This model was developed under the tested assumption of log-normality of the equivalent number of cycles.

Fig. 9 shows the residuals against the predictor variables used in Eq. (2) for Zone 602, as an example. The same comments made in regards to the residual plots for the  $r_{d-Gron}$  model (Fig. 7) also apply

to the residual plots for the  $n_{eqM-Gron}$  model shown in Fig. 9. In interpreting the residual plots shown in both Figs. 7 and 9, it needs to be realized that any of the small biases that may be observed are smaller than the standard deviations of the binned residuals.

Although the worldwide model for  $n_{eq}$  developed by Lasley et al. (2017) included a depth dependence of the standard deviation, there is no compelling evidence of this in the Groningen datasets [Fig. 9(d)]. Accordingly, a homoscedastic standard deviation (i.e., independent of predictor variables) was adopted for the Groningen-zone-specific model.

Consistent with the revised MSF relationship given in Green et al. (2019), the Groningen-zone-specific MSF relationship is given by the following expression:



**Fig. 10.** (Color) Comparison of MSF relationships proposed by Idriss and Boulanger (2008) ( $MSF_{IB08}$ ) and Green et al. (2019) ( $MSF_{WUS}$ ), and Groningen-specific relationship ( $MSF_{Gron}$ ) for Zone 602. Because  $MSF_{WUS}$  and  $MSF_{Gron}$  are functions of  $a_{max}$ , curves for  $a_{max} = 0.1, 0.2,$  and  $0.3g$  are shown in the plots.

$$MSF_{Gron} = \left\{ \frac{7.25}{n_{eqM-Gron}(M, a_{max}, V_{s12})} \right\}^{0.34} \leq 2.04 \quad (3a)$$

and

$$\sigma_{\ln(MSF_{Gron})} = 0.34 \cdot \sigma_{\ln(n_{eqM-Gron})} \quad (3b)$$

where the denominator in Eq. (3a) is computed using Eq. (2). Also, note that the numerator in Eq. (3a) differs from that used by Green et al. (2019) for the revised worldwide MSF (i.e., 7.25 versus 14). The reason for this is that the revised worldwide MSF relationship was derived using both horizontal components of motions recorded at a site during tectonic events and Eq. (3a) was derived using single components of motions generated using a seismic source model, as discussed. Accordingly, 7.25 represents the reference number of equivalent cycles for one horizontal component of motion for an  $M = 7.5$  event in active shallow tectonic seismic zones and is computed using the relationship given in Lasley et al. (2017), Approach 1, WUS:  $M = 7.5$  and  $a_{max} = 0.35g$ . The cap of 2.04 on  $MSF_{Gron}$  corresponds to a motion composed of one, low amplitude pulse in one of the horizontal components of motion.

Fig. 10 shows a comparison of the Groningen-specific MSF relationship for Zone 602, as an example, and the worldwide relationships proposed by Idriss and Boulanger (2008) ( $MSF_{IB08}$ ) and Green et al. (2019) ( $MSF_{WUS}$ ). As shown in Fig. 10, the  $MSF_{IB08}$  relationship predicts significantly larger values for magnitudes less than  $M \sim 7.0$ , with the overprediction being more significant as magnitude decreases. However, the  $MSF_{WUS}$  and  $MSF_{Gron}$  do not differ significantly across magnitude, with the  $MSF_{Gron}$  showing a slightly less dependence on  $a_{max}$ .

### Correlations between Groningen-Zone-Specific $r_d$ and $\ln(n_{eq})$ Relationships

The results show that  $r_{d-Gron}$  is correlated across depths and that  $\ln(n_{eqM-Gron})$  and  $r_{d-Gron}$  are negatively correlated at a given depth. The correlation coefficient of  $r_{d-Gron}$  at depths  $z_i$  and  $z_j$  is given by the following expression

$$\rho[\varepsilon_{r_{d-Gron}}(z_i), \varepsilon_{r_{d-Gron}}(z_j)] = 1 + \alpha_{r_{d-Gron}} \cdot |z_i - z_j| \quad (4)$$

**Table 4.** Correlation coefficients for  $r_{d-Gron}$  and  $\ln(n_{eqM-Gron})$  models

Zone	$\alpha_{r_{d-Gron}}$	$\rho_{\ln(n_{eqM-Gron}), r_{d-Gron}}$
602	-0.0427	-0.2474
603	-0.0385	-0.3169
604	-0.0340	-0.3917
801	-0.0355	-0.3152
821	-0.0304	-0.3266
1001	-0.0486	-0.2627
1032	-0.0499	-0.2659
2001	-0.0495	-0.3881
Zandeweer	-0.0365	-0.3113

where  $\varepsilon_{r_{d-Gron}}$  = number of standard deviations from the median  $r_{d-Gron}$  value;  $z_{i,j}$  are in m; and  $\alpha_{r_{d-Gron}}$  is dimensionless (Table 4). Also, the correlation coefficients for  $\ln(n_{eqM-Gron})$  and  $r_{d-Gron}$  (i.e.,  $\rho_{\ln(n_{eqM-Gron}), r_{d-Gron}}$ ) are listed in Table 4.

In the next section, the Groningen-specific relationships,  $r_{d-Gron}$  and  $MSF_{Gron}$ , in conjunction with the revised CRR curve (Green et al. 2019), are used to assess the liquefaction hazard across the Groningen liquefaction study area shown in Fig. 6.

### Groningen Liquefaction Hazard

Liquefaction hazard curves were calculated for 95 sites across the study area using a Monte Carlo approach. The probability distributions for seismic activity rates (Bourne and Oates 2017), event locations and magnitudes, and resulting ground motions were sampled such that the simulated future seismic hazard is consistent with historical seismic and reservoir-compaction datasets (Bourne et al. 2015) up to a maximum event, which its size is defined by a logic-tree (Bommer and van Elk 2017). The ground motions are predicted using the ground motion model described in Bommer et al. (2017a). The ground motion model was developed following the scheme described in Bommer et al. (2017b) and summarized previously herein is used to generate ground motions for multiple scenarios (e.g., multiple magnitude and distance combinations) at

the NS\_B horizon. Period-, intensity-, and scenario-dependent amplification factors (median values and standard deviations) for each of the zones in the Groningen region (e.g., Fig. 6) were used to convert the NS\_B motions to surface ground motions (Rodriguez-Marek et al. 2017; Stafford et al. 2017).

For each event scenario, the Groningen-specific relationships,  $r_{d-Gron}$  and  $MSF_{Gron}$ , in conjunction with the revised CRR curve (Green et al. 2019), were used to compute the  $FS_{liq}$  as a function of depth. All other relationships required to compute  $FS_{liq}$  were adopted from Boulanger and Idriss (2014), consistent with the development of the revised CRR curve. The  $LPI_{ish}$  framework (Maurer et al. 2015b) was used to relate the computed  $FS_{liq}$  in strata at depth in a profile to the predicted severity of surficial liquefaction manifestations, which has been shown to correlate to the liquefaction damage potential for level-ground sites (e.g., Iwasaki et al. 1978; Tonkin and Taylor 2013). The  $LPI_{ish}$  framework is a conceptual and mathematical merger of the Ishihara (1985)  $H_1$ - $H_2$  chart and liquefaction potential index (LPI) framework (Iwasaki et al. 1978), resulting in a framework that is relatively easy to implement for profiles having varying stratigraphies (where the major limitation of the Ishihara  $H_1$ - $H_2$  chart is that it can only be applied to profiles having relatively simple stratigraphies, as discussed in the following section) and better accounts for the thickness of the nonliquefiable crust on the severity of surficial liquefaction manifestations than the LPI framework (e.g., Green et al. 2018b). As detailed in Maurer et al. (2015b),  $LPI_{ish}$  index values are functions of the thickness of the nonliquefiable crust, cumulative thickness of liquefied layers, proximity of these layers to the ground surface, and amount by which  $FS_{liq}$  in each layer is less than 1.0.

The optimal  $LPI_{ish}$  thresholds corresponding to different severities of surficial liquefaction manifestations are dependent on the liquefaction triggering procedure used to compute  $FS_{liq}$  and the characteristics of the profile; the same is true for other liquefaction damage severity frameworks (Maurer et al. 2015a). However, without liquefaction case history data to develop Groningen-specific thresholds, the thresholds proposed by Iwasaki et al. (1978) for the LPI framework were conservatively (Maurer et al. 2015a) used

in this study with the  $LPI_{ish}$  framework i.e.:  $LPI_{ish} < 5$ : no to minor surficial liquefaction manifestations;  $5 \leq LPI_{ish} \leq 15$ : moderate surficial liquefaction manifestations;  $LPI_{ish} > 15$ : severe surficial liquefaction manifestations.

The output from the liquefaction study is a set of liquefaction hazard curves for the 95 sites across the liquefaction study area, where the hazard curves show the AFE for varying  $LPI_{ish}$  values for a site. Example curves computed for two sites, one in Zone 602 and one in Zandeweer, are shown in Fig. 11; Zone 602 is representative of most of the zones across the liquefaction study area, except for Zandeweer, which has the highest computed liquefaction hazard of all the zones. Consistent with the requirements of NPR 9998-2017 (NPR 2017),  $LPI_{ish}$  values corresponding to an AFE of  $\sim 4 \times 10^{-4}$  (or a 2475-year return period) are of most interest. However, the previous version of the NPR 9998 (NPR 2015) specified an 800-year return period for evaluating the liquefaction potential for CC1b type structures (i.e., 1, 2, or 3-story single family homes, agriculture buildings, greenhouses, and 1- or 2-story industrial buildings), which was used as the basis for a previous liquefaction hazard study of Zandeweer (Kumar 2017). Also, both the 2015 and 2017 versions of the NPR 9998 reference the IB08 liquefaction triggering model. As a result, Fig. 11 also shows the AFE corresponding to an 800-year return period and the  $LPI_{ish}$  hazard curves computed using IB08. The liquefaction hazard curves for all 95 sites across the liquefaction study area, grouped by zones, are presented in Green et al. (2018a).

As may be observed from Fig. 11, use of the Groningen-specific liquefaction model in the PLHA results in a higher computed liquefaction hazard for a 2475-year return period than when IB08 is used; this was the case for all sites evaluated. Additionally,  $LPI_{ish} < 5$ : no to minor surficial liquefaction manifestations are predicted for an 800-year return period for both sites when both the Groningen-specific and IB08 liquefaction triggering models are used in the PLHA; this again was the case for all sites evaluated. For a 2475-year return period,  $LPI_{ish} < 5$ : no to minor surficial liquefaction manifestations are predicted for both sites when IB08 is used in the PLHA (this was the case for all sites) and for Zone 602 site when the Groningen-specific model is used in the PLHA.

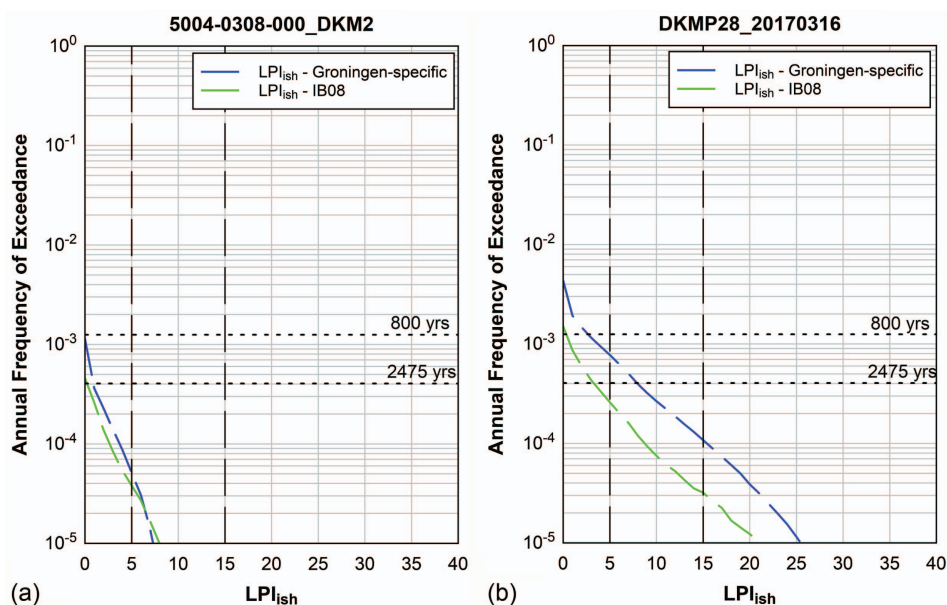


**Fig. 11.** (Color) Liquefaction hazard curves computed for sites in (a) Zone 602; and (b) Zone Zandeweer. Zone 602 is representative of most of the zones across the liquefaction study area, except for Zandeweer, which had the highest computed liquefaction hazard.

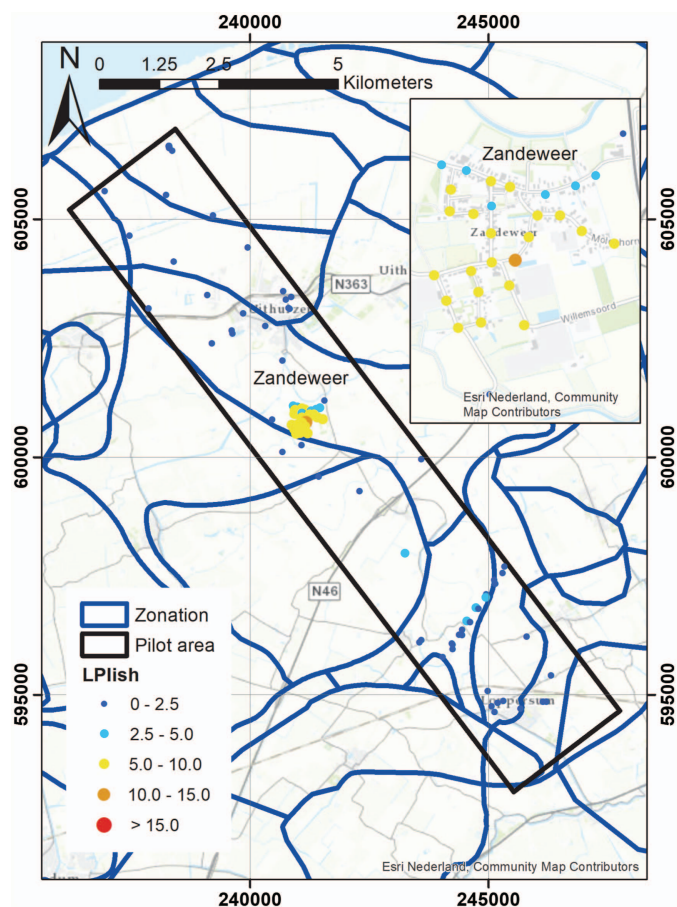


**Fig. 12.** (Color) Liquefaction hazard map for 2475-year return period computed using the Groningen-specific liquefaction evaluation procedure for the entire liquefaction study area and for Zandeweer (inset). (© Esri Nederland, Community Map Contributors.)

However,  $LPI_{ish} \sim 8$  (i.e., moderate surficial liquefaction manifestations) is predicted for a 2475-year return period for the Zandeweer site when the Groningen-specific model is used in the PLHA; this is the case for 21 of the 27 sites evaluated in Zandeweer.

Fig. 12 shows liquefaction hazard maps for a 2475-year return period computed using the Groningen-specific model in the PLHA for the entire liquefaction study area and for Zandeweer. The only sites in the liquefaction study area that are predicted to have moderate surficial liquefaction manifestations are all located in Zandeweer [Fig. 12(b)]; all other sites in the study area have  $LPI_{ish} < 5$ .

## Conclusions

Although an almost negligible contributor to earthquake fatalities, liquefaction triggering is an important threat to the built environment and in particular to infrastructure and lifelines and is thus being included as part of the seismic hazard and risk study of the Groningen region being directed by NAM. Due to the unique characteristics of both the seismic hazard and the geologic profiles/soil deposits in Groningen, direct application of existing liquefaction triggering models in the study was deemed inappropriate and was shown to be so by comparing  $r_d$  and MSF relationships inherent to existing triggering models with Groningen-specific relationships developed as part of this study. A PLHA was performed using a

Monte Carlo method wherein probability distributions for seismic activity rates, event locations and magnitudes, and resulting ground motions are sampled such that the simulated future seismic hazard is consistent with historical seismic and reservoir-compaction datasets up to a maximum event, the size of which is defined by a logic-tree distribution. The differences between the Groningen-specific and the NPR 9998-2017 specified IB08 liquefaction triggering models manifest in the computed liquefaction hazard curves (i.e., AFE versus  $LPI_{ish}$ ) for sites across the study area, with the predicted liquefaction hazard generally being higher when the Groningen-specific liquefaction triggering model is used in the PLHA.

Consistent with the requirements of NPR 9998-2017,  $LPI_{ish}$  values corresponding to an AFE of  $\sim 4 \times 10^{-4}$  (or a 2475-year return period) are of particular interest. However, assessing the liquefaction hazard by determining the  $LPI_{ish}$  values for the specified return period goes well beyond the requirements of NPR 9998-2017 (as well as all other building codes that the authors are familiar with), which allows a pseudo-probabilistic approach to be employed (i.e., assessing the liquefaction triggering potential for a ground motion having a 2475-year return period). Additionally, the integration of the liquefaction hazard study within the broader regional seismic hazard study resulted in one of the most comprehensive PLHA performed to date globally due to the development and use of a regional stochastic source model, GMPE, site response model, and geologic model, as well as the region-specific liquefaction model (refer to Fig. 1). The  $LPI_{ish}$  values for the vast majority of the sites across the study area are less than 5, indicating no to minor surficial liquefaction manifestations. The only sites within the study area that had  $LPI_{ish}$  values greater than 5, which is the threshold between no to minor surficial liquefaction manifestations and moderate surficial liquefaction manifestations, were in Zandeweer, with only some of the sites in Zandeweer exceeding this threshold value. No sites across the study are predicted to have severe surficial liquefaction manifestations.

Finally, mention is needed regarding two phenomena that were not considered in the liquefaction study presented in this paper: the influence of sand age on liquefaction triggering resistance (i.e., aging effects) and the influence of thin layer effects on measured CPT tip resistance (i.e., thin layer effects). Investigations into both of these phenomena were being performed in parallel with the work presented in this paper, with the efforts lead by colleagues at Deltares. The Deltares' studies were not far enough along to be incorporated into the analyses presented herein. However, it should be noted that ignoring both aging and thin layer effects likely results in an overprediction of liquefaction hazard (i.e., the hazard estimates presented herein may be considered conservative), but the extent of the possible overprediction is unknown at this time.

## Acknowledgments

This research was partially funded by Nederlandse Aardolie Maatschappij B.V. (NAM) and the National Science Foundation (NSF) Grants CMMI-1435494, CMMI-1724575, CMMI-1825189, and CMMI-1937984. This support is gratefully acknowledged. This study has also significantly benefited from enlightening discussions with colleagues at Shell, Deltares, Arup, Fugro, Beca, and on the Netherlands Normalisatie Instituut (NEN) Liquefaction Task Force, which is coordinated by Dr. Mandy Korff. However, any opinions, findings, and conclusions or recommendations expressed in this material are those of the authors and do not necessarily reflect the views of the NSF, NAM, or others that are acknowledged.

## References

- Anderson, J. G., and S. E. Hough. 1984. "A model for the shape of the Fourier amplitude spectrum of acceleration at high frequencies." *Bull. Seismol. Soc. Am.* 74 (5): 1969–1993.
- Bird, J. F., and J. J. Bommer. 2004. "Earthquake losses due to ground failure." *Eng. Geol.* 75 (2): 147–179. <https://doi.org/10.1016/j.enggeo.2004.05.006>.
- Boatwright, J. 1978. "Detailed spectral analysis of two small New York state earthquakes." *Bull. Seismol. Soc. Am.* 68 (4): 1117–1131.
- Bommer, J. J., et al. 2017a. *V4 Ground-Motion Model (GMM) for response spectral accelerations, peak ground velocity, and significant durations in the Groningen field. Version 2.1*. Assen, Netherlands: Nederlandse Aardolie Maatschappij B.V.
- Bommer, J. J., B. Dost, B. Edwards, P. J. Stafford, J. van Elk, D. Doornhof, and M. Ntinalexis. 2016. "Developing an application-specific ground-motion model for induced seismicity." *Bull. Seismol. Soc. Am.* 106 (1): 158–173. <https://doi.org/10.1785/0120150184>.
- Bommer, J. J., P. J. Stafford, B. Edwards, and B. Dost. 2017b. "Framework for a ground-motion model for induced seismic hazard and risk analysis in the Groningen gas field, the Netherlands." *Earthquake Spectra* 33 (2): 481–498. <https://doi.org/10.1193/082916EQS138M>.
- Bommer, J. J., and J. van Elk. 2017. "Comment on 'The maximum possible and the maximum expected earthquake magnitude for production-induced earthquakes at the gas field in Groningen, the Netherlands' by Gert Zöller and Matthias Holschneider." *Bull. Seismol. Soc. Am.* 107 (3): 1564–1567. <https://doi.org/10.1785/0120170040>.
- Boore, D. M. 2009. "Comparing stochastic point-source and finite-source ground-motion simulations: SMSIM and EXSIM." *Bull. Seismol. Soc. Am.* 99 (6): 3202–3216. <https://doi.org/10.1785/0120090056>.
- Boulanger, R. W., and I. M. Idriss. 2014. *CPT and SPT based liquefaction triggering procedures*. Rep. No. UCDC/CGM-14/01. Davis, CA: Univ. of California at Davis.
- Bourne, S. J., and S. J. Oates. 2017. "Extreme threshold failures within a heterogeneous elastic thin-sheet account for the spatial-temporal development of induced seismicity within the Groningen gas field." *J. Geophys. Res. Solid Earth* 122 (12): 10299–10320.
- Bourne, S. J., S. J. Oates, J. J. Bommer, B. Dost, J. van Elk, and D. Doornhof. 2015. "A Monte Carlo method for probabilistic seismic hazard assessment of induced seismicity due to conventional gas production." *Bull. Seismol. Soc. Am.* 105 (3): 1721–1738. <https://doi.org/10.1785/0120140302>.
- Brune, J. N. 1970. "Tectonic stress and the spectra of seismic shear waves from earthquakes." *J. Geophys. Res.* 75 (26): 4997–5009. <https://doi.org/10.1029/JB075i026p04997>.
- Cetin, K. O. 2000. "Reliability-based assessment of seismic soil liquefaction initiation hazard." Ph.D. thesis, Dept. of Civil and Environmental Engineering, Univ. of California at Berkeley.
- Edwards, B., B. Zurek, E. van Dedem, P. J. Stafford, S. Oates, J. van Elk, B. deMartin, and J. J. Bommer. 2019. "Simulations for the development of a ground motion model for induced seismicity in the Groningen gas field, The Netherlands." *Bull. Earthquake Eng.* 17 (8): 4441–4456. <https://doi.org/10.1007/s10518-018-0479-5>.
- Green, R. A., et al. 2018a. *Liquefaction hazard pilot study for the Groningen region of the Netherlands due to induced seismicity*, edited by J. van Elk, and D. Doornhof, 175. Nederlandse Aardolie Maatschappij B.V.
- Green, R. A., and J. J. Bommer. 2019. "What is the smallest earthquake magnitude that needs to be considered in assessing liquefaction hazard?" *Earthquake Spectra* 35 (3): 1441–1464. <https://doi.org/10.1193/032218EQS064M>.
- Green, R. A., J. J. Bommer, A. Rodriguez-Marek, B. Maurer, P. Stafford, B. Edwards, P. P. Kruiver, G. de Lange, and J. van Elk. 2019. "Addressing limitations in existing 'simplified' liquefaction triggering evaluation procedures: Application to induced seismicity in the Groningen gas field." *Bull. Earthquake Eng.* 17 (8): 4539–4557. <https://doi.org/10.1007/s10518-018-0489-3>.
- Green, R. A., B. W. Maurer, and S. van Ballegooy. 2018b. "The influence of the non-liquefied crust on the severity of surficial liquefaction manifestations: Case history from the 2016 Valentine's Day earthquake in New Zealand." In Vol. 290 of *Proc. Geotechnical Earthquake Engineering and Soil Dynamics V (GEESD V), Liquefaction Triggering, Consequences, and Mitigation*, edited by S. J. Brandenberg and M. T. Manzari, 21–32. Reston, VA: ASCE Geotechnical Special Publication.
- Hakuno, M. 2004. "Ground liquefaction is not dangerous for human lives." In *Proc. 13th World Conf. on Earthquake Engineering* Tokyo: International Association for Earthquake Engineering.
- Idriss, I. M. 1999. "An update to the Seed-Idriss simplified procedure for evaluating liquefaction potential." In *Proc. TRB Workshop on New Approaches to Liquefaction*, Publication No. FHWA-RD-99-165. Washington, DC: Federal Highway Administration.
- Idriss, I. M., and R. W. Boulanger. 2008. *Soil liquefaction during earthquakes, Monograph MNO-12*. Oakland, CA: Earthquake Engineering Research Institute.
- Ishihara, K. 1985. "Stability of natural deposits during earthquakes" In vol. 1 of *Proc. 11th Int. Conf. on Soil Mechanics and Foundation Engineering*, 321–376. London, UK: International Society of Soil Mechanics and Geotechnical Engineering.
- Iwasaki, T., F. Tatsuoka, K. Tokida, and S. Yasuda. 1978. "A practical method for assessing soil liquefaction potential based on case studies at various sites in Japan." In *Proc. 2nd Int. Conf. on Microzonation*. San Francisco, CA: National Science Foundation, UNESCO, ASCE, Earthquake Engineering Research Institute, Seismological Society of America, Universities Council for Earthquake Engineering Research.
- Kayen, R., R. E. S. Moss, E. M. Thompson, R. B. Seed, K. O. Cetin, A. Der Kiureghian, Y. Tanaka, and K. Tokimatsu. 2013. "Shear-wave velocity-based probabilistic and deterministic assessment of seismic soil liquefaction potential." *J. Geotech. Geoenviron. Eng.* 139 (3): 407–419. [https://doi.org/10.1061/\(ASCE\)GT.1943-5606.0000743](https://doi.org/10.1061/(ASCE)GT.1943-5606.0000743).
- Korff, M., P. Meijers, A. Wiersma, and F. Kloosterman. 2019. "Mapping liquefaction based on CPT data for induced seismicity in Groningen." In *Proc. 7th Int. Conf. on Earthquake Geotechnical Engineering (7ICEGE)*. London, UK: International Society of Soil Mechanics and Geotechnical Engineering.
- Kottke, A. R., and E. M. Rathje. 2008. *Technical manual for STRATA*. PEER Report 2008/10. Berkeley, CA: Pacific Earthquake Engineering Center, Univ. of California at Berkeley.
- Kruiver, P. P., et al. 2017a. "An integrated shear-wave velocity model for the Groningen gas field, The Netherlands." *Bull. Earthquake Eng.* 15 (9): 3555–3580. <https://doi.org/10.1007/s10518-017-0105-y>.
- Kruiver, P. P., et al. 2017b. "Characterisation of the Groningen subsurface for seismic hazard and risk modeling." *Neth. J. Geosci.* 96 (5): s215–s233. <https://doi.org/10.1017/njg.2017.11>.
- Kumar, P. 2017. *Zandeweer areal approach ground models and liquefaction assessment*. Rep. No. 229746\_048.0\_REP2064\_Rev0.01. Amsterdam, Netherlands: Centrum Veilig Wonen (CVW), Arup bv.
- Lasley, S., R. A. Green, and A. Rodriguez-Marek. 2016. "A new stress reduction coefficient relationship for liquefaction triggering analyses." *J. Geotech. Geoenviron. Eng.* 142 (11): 06016013. [https://doi.org/10.1061/\(ASCE\)GT.1943-5606.0001530](https://doi.org/10.1061/(ASCE)GT.1943-5606.0001530).
- Lasley, S., R. A. Green, and A. Rodriguez-Marek. 2017. "Number of equivalent stress cycles for liquefaction evaluations in active tectonic and stable continental regimes." *J. Geotech. Geoenviron. Eng.* 143 (4): 04016116. [https://doi.org/10.1061/\(ASCE\)GT.1943-5606.0001629](https://doi.org/10.1061/(ASCE)GT.1943-5606.0001629).
- Lunne, T., P. K. Robertson, and J. J. M. Powell. 1997. *Cone penetration testing in geotechnical practice*. London: EF Spon/Blackie Academic, Routledge Publishers.
- Maurer, B. W., R. A. Green, M. Cubrinovski, and B. A. Bradley. 2015a. "Fines-Content effects on liquefaction hazard evaluation for infrastructure in Christchurch, New Zealand." *Soil Dyn. Earthquake Eng.* 76 (Sep): 58–68. <https://doi.org/10.1016/j.soildyn.2014.10.028>.
- Maurer, B. W., R. A. Green, and O.-D. S. Taylor. 2015b. "Moving towards an improved index for assessing liquefaction hazard: Lessons from historical data." *Soils Found.* 55 (4): 778–787. <https://doi.org/10.1016/j.sandf.2015.06.010>.
- Moss, R. E. S., R. B. Seed, R. E. Kayen, J. P. Stewart, T. L. Youd, and K. Tokimatsu. 2003. *Field case histories for CPT-based in situ liquefaction potential evaluation*. Geoenvironment Research Report UCB/GE-2003/04. Berkeley, CA: Univ. of California, Berkeley.

- Motazedian, D., and G. M. Aktinson. 2005. "Stochastic finite-fault modelling based on a dynamic corner frequency." *Bull. Seismol. Soc. Am.* 95 (3): 995–1010. <https://doi.org/10.1785/0120030207>.
- NAM (Nederlandse Aardolie Maatschappij B.V.). 2019. "Earthquakes (Gr.), Nederlandse Aardolie Maatschappij B.V. (NAM)." Accessed October 18, 2019. [https://www.nam.nl/feiten-en-cijfers/aardbevingen.html#iframe=L2VtYmVkL2NvbXBvbmVudC8\\_aWQ9YWYfZGJldmluZ2Vu](https://www.nam.nl/feiten-en-cijfers/aardbevingen.html#iframe=L2VtYmVkL2NvbXBvbmVudC8_aWQ9YWYfZGJldmluZ2Vu).
- Noorlandt, R. P., et al. 2018. "Characterisation of ground-motion recording stations in the Groningen gas field." *J. Seismolog.* 22 (3): 605–623. <https://doi.org/10.1007/s10950-017-9725-6>.
- NPR (Nationale Praktijk Richtlijn). 2015. *Assessment of buildings in case of erection, reconstruction and disapproval—Basic rules for seismic actions: Induced earthquakes*. NPR 9998. Delft, Netherlands: Netherlands Normalisatie Instituut.
- NPR (Nationale Praktijk Richtlijn). 2017. *Assessment of structural safety of buildings in case of erection, reconstruction and disapproval—Basis rules for seismic actions: Induced earthquakes*. NPR 9998. Delft, Netherlands: Netherlands Normalisatie Instituut.
- NRC (National Research Council). 2016. "State of the art and practice in the assessment of earthquake-induced soil liquefaction and consequences." In *Committee on earthquake induced soil liquefaction assessment*, edited by E. Kavazanjian, Jr., et al. Washington, DC: NRC, The National Academies Press.
- Rodriguez-Marek, A., P. P. Kruiver, P. Meijers, J. J. Bommer, B. Dost, J. van Elk, and D. Doornhof. 2017. "A regional site-response model for the Groningen gas field." *Bull. Seismol. Soc. Am.* 107 (5): 2067–2077.
- Stafford, P. J., A. Rodriguez-Marek, B. Edwards, P. P. Kruiver, and J. J. Bommer. 2017. "Scenario dependence of linear site effect factors for short-period response spectral ordinates." *Bull. Seismol. Soc. Am.* 107 (6): 2859–2872. <https://doi.org/10.1785/0120170084>.
- Stafleu, J., D. Maljers, J. L. Gunnink, A. Menkovic, and F. S. Busschers. 2011. "3D modelling of the shallow subsurface of Zeeland, the Netherlands." *Neth. J. Geosci.* 90 (4): 293–310. <https://doi.org/10.1017/S0016774600000597>.
- Thum, T. S., S. Lasley, R. A. Green, and A. Rodriguez-Marek. 2019. *ShakeVT2: A computer program for equivalent linear site response analysis*, Center for Geotechnical Practice and Research (CGPR) Report #98, The Charles E. Via, Jr. Blacksburg, VA: Dept. of Civil and Environmental Engineering, Virginia Tech.
- Tonkin and Taylor. 2013. *Liquefaction vulnerability study, Report prepared for the Earthquake Commission*. Auckland, New Zealand: Tonkin & Taylor LTD.
- Trifonov, V. G., J. Klerkx, and K. Theunissen. 1994. "The Roermond earthquake of 13 April 1992, the Netherlands: Geological aspects." *Terra Nova* 6 (3): 301–305. <https://doi.org/10.1111/j.1365-3121.1994.tb00500.x>.
- van Eck, T., F. Goutbeek, H. Haak, and B. Dost. 2006. "Seismic hazard due to small-magnitude, shallow source, induced earthquakes in the Netherlands." *Eng. Geol.* 87 (1–2): 105–121. <https://doi.org/10.1016/j.enggeo.2006.06.005>.
- van Elk, J., S. J. Bourne, S. J. Oates, J. J. Bommer, R. Pinho, and H. Crowley. 2019. "A probabilistic model to evaluate options for mitigating induced seismic risk." *Earthquake Spectra* 35 (2): 537–564. <https://doi.org/10.1193/050918EQS118M>.
- van Elk, J., D. Doornhof, J. J. Bommer, S. J. Bourne, S. J. Oates, R. Pinho, and H. Crowley. 2017. "Hazard and risk assessments for induced seismicity in Groningen." *Neth. J. Geosci.* 96 (5): s259–s269. <https://doi.org/10.1017/njg.2017.37>.
- Wells, D. L., and K. J. Coppersmith. 1994. "New empirical relationships among magnitude, rupture length, rupture width, rupture area, and surface displacement." *Bull. Seismol. Soc. Am.* 84 (4): 974–1002.